frontiers | Frontiers in Materials

TYPE Original Research
PUBLISHED 30 October 2024
DOI 10.3389/fmats.2024.1470878

OPEN ACCESS

EDITED BY
Alberto De La Torre,
Northeastern University, United States

REVIEWED BY
John Harter,
University of California, Santa Barbara, United States
Badih A. Assaf,
University of Notre Dame, United States

*CORRESPONDENCE
Eteri Svanidze,
eteri.svanidze@cpfs.mpg.de

RECEIVED 26 July 2024
ACCEPTED 03 October 2024
PUBLISHED 30 October 2024

CITATION
Nixon R, Prots Y, Krnel M, Zaremba N, Pavlosiuk O, Schmidt M, Akselrud L, Grin Y and Svanidze E (2024) Superconductivity in mercurides of strontium.
Front. Mater. 11:1470878.
doi: 10.3389/fmats.2024.1470878

Superconductivity in mercurides of strontium

Rachel Nixon[1,2], Yurii Prots[1], Mitja Krnel[1], Nazar Zaremba[1], Orest Pavlosiuk[3], Marcus Schmidt[1], Lev Akselrud[1,4], Yuri Grin[1] and Eteri Svanidze[1]*

[1]Max Planck Institute for Chemical Physics of Solids, Dresden, Germany, [2]University of St Andrews, Fife, United Kingdom, [3]Institute of Low Temperature and Structure Research, Polish Academy of Sciences, Wrocław, Poland, [4]Ivan Franko Lviv National University, Lviv, Ukraine

A large variety of chemical and physical properties are exhibited by mercurides and amalgams. In this work, we have successfully examined seven strontium mercurides: $SrHg_{11}$, $SrHg_8$, $Sr_{10}Hg_{55}$, $SrHg_2$, SrHg, Sr_3Hg_2, and Sr_3Hg. The interest in the mercury-rich region is motivated by the large number of mercury-based superconductors that have high mercury content. At the same time, the preparation on the mercury-rich side of the binary phase diagram is experimentally non-trivial, due to the high vapor pressure of mercury and extreme air-sensitivity of mercury-rich compounds. By employing a set of specialized techniques, we were able to discover superconductivity in three mercury-strontium compounds – $SrHg_{11}$ ($T_c = 3.2 \pm 0.3$ K, $H_{c2} = 0.18 \pm 0.05$ T), $SrHg_8$ ($T_c = 3.0 \pm 0.1$ K, $H_{c2} = 0.35 \pm 0.02$ T), and $Sr_{10}Hg_{55}$ ($T_c = 2.2 \pm 0.25$ K, $H_{c2} = 0.54 \pm 0.05$ T).

KEYWORDS

amalgams, mercurides, superconductivity, mercury, strontium, phase diagram, noncentrosymmetry

1 Introduction

Mercury-based compounds (mercurides) and mercury-based alloys (amalgams) have long been of significant interest in chemistry and physics (Ferro, 1954; Bruzzone and Merlo, 1973; Bruzzone and Merlo, 1974; Bruzzone and Merlo, 1975). From their everyday applications (Bjørklund, 1989; Sappl et al., 2017) to their unique superconducting and topological states (Pelloquin et al., 1993; König et al., 2007), a plethora of exciting phenomena emerge in these systems. Many mercury-based materials have unique and complex crystal structures (Tkachuk and Mar, 2008), and it is suggested that the complexity of these structures is directly related to their intriguing physical properties (Steurer and Dshemuchadse, 2016; Dubois and Belin-Ferré, 2010; Urban and Feuerbacher, 2004; Conrad et al., 2009; Samson, 1962; Weber et al., 2009; Svanidze et al., 2019; Prots et al., 2022b). Among the alkali- and alkali-earth-based mercurides, a large variety of crystallographic motifs was observed with almost 40 structure types present, ranging in complexity from simple CsCl structure type (2 atoms per unit cell, Pearson symbol $\bar{c}P2$) to the exceptionally complex $Sm_{11}Cd_{45}$ structure type (448 atoms per unit cell, Pearson symbol $cF448$). Despite these fascinating atomic environments and peculiar physical properties, an overwhelming majority of mercury-based systems

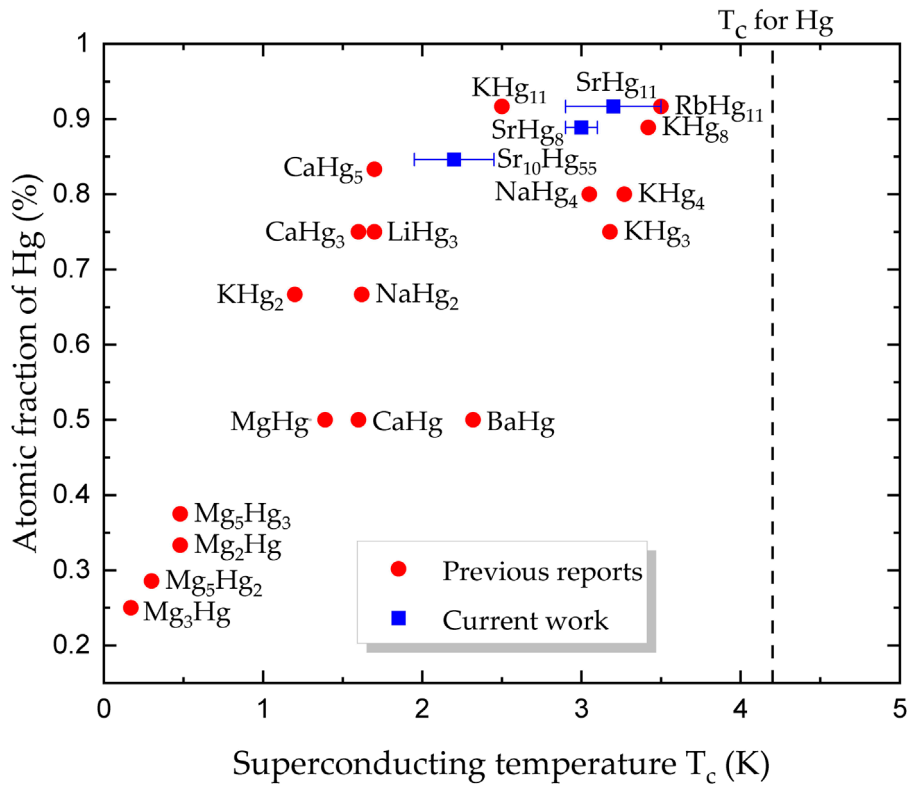

FIGURE 1
Binary superconductors containing mercury and alkali or alkali-earth elements. Superconductors reported as part of this work are marked with blue squares, while those reported previously are shown as red circles (Claeson and Luo, 1966; Roberts, 1976; Biehl and Deiseroth, 1999; Claeson and Luo, 1966; Hohl et al., 2023; Hänisch et al., 2023). The maximum value for the superconducting temperature T_c appears to be slightly below that of pure Hg (T_c = 4.2 K).

have not been studied in detail – likely due to the difficulties associated with such work (Bjørklund et al., 2017; Hoch, 2019). Moreover, their extreme air- and moisture-sensitivity (Witthaut et al., 2023; Prots et al., 2022a; Prots et al., 2022b), call for a specialized preparation methodology.

The first analysis of mercury-strontium compounds and amalgams was carried out in the end of 19th century (Kerp, 1898; Kerp et al., 1900; Guntz and Roederer, 1906; Devoto and Recchia, 1930), with the first study of crystal structure dating back to 1954 (Ferro, 1954). The binary phase diagram was first unified 20 years later (Bruzzone and Merlo, 1974), and re-evaluated in 2005 (Gumiński, 2005), resulting in reformulation of multiple phases (Kerp et al., 1900; Guntz and Roederer, 1906; Devoto and Recchia, 1930). Both mercurides as well as isostructural families of compounds have been studied after that: for example, Sr_3Hg_2 (Druska et al., 1996), AHg_{11} (A = K, Rb, Ba or Sr) (Biehl and Deiseroth, 1999), $SrHg_3$ (Wendorff and Röhr, 2018), and $A_{11-x}Hg_{54+x}$ (A = Ca or Sr) (Tkachuk and Mar, 2008). The aforementioned work on the mercury-strontium compounds has so far focused on the chemical features of these compounds (Ferro, 1954; Kerp et al., 1900; Guntz and Roederer, 1906; Devoto and Recchia, 1930; Biehl and Deiseroth, 1999; Wendorff and Röhr, 2018), leaving the physical properties unknown. Our previous work on mercurides revealed a number of new superconducting (Prots et al., 2022a; Witthaut et al., 2023) and magnetic (Svanidze et al., 2019; Prots et al., 2022b) compounds, which motivated us to re-assess the mercury-strontium binary system. In the current work, we have successfully synthesized $SrHg_{11}$, $SrHg_8$, $Sr_{10}Hg_{55}$, $SrHg_2$, SrHg, Sr_3Hg_2, and Sr_3Hg. The mercury-rich compounds $SrHg_{11}$, $SrHg_8$, and $Sr_{10}Hg_{55}$ were synthesized in single-crystalline form. Despite their exceptional air-sensitivity, it was possible to conclusively establish that these compounds exhibit superconductivity with critical temperatures $Sr_{10}Hg_{55}$ ($T_c = 2.2 \pm 0.25$ K), $SrHg_8$ ($T_c = 3.0 \pm 0.1$ K), and $SrHg_{11}$ ($T_c = 3.2 \pm 0.3$ K), respectively. The other mercury-strontium phases are para- or diamagnetic down to $T = 1.8$ K. This work expands the number of currently known superconducting alkali- or alkali-earth-based mercurides, as summarized in Figure 1 (Claeson and Luo, 1966; Roberts, 1976; Biehl and Deiseroth, 1999; Claeson and Luo, 1966; Hohl et al., 2023; Hänisch et al., 2023).

2 Materials and methods

Several issues complicate experimental investigations of mercury-containing materials – toxicity, high vapor pressure, high chemical reactivity, and extreme air sensitivity – call for a specialized laboratory environment. As we have previously shown (Witthaut et al., 2023; Prots et al., 2022a; Prots et al., 2022b; Svanidze et al., 2019), it is possible to conclusively establish chemical

10.3389/fmats.2024.1470878

TABLE 1 Summary of phase analysis in mercury-strontium samples, synthesized as part of this work.

Sample number	Starting composition	Sample form	Main phase	Secondary phase
1	Sr_3Hg_{97}	single crystal	$SrHg_{11}$	$SrHg_8$
2	Sr_3Hg_{97}	single crystal	$SrHg_{11}$	$SrHg_8$
3	Sr_3Hg_{97}	single crystal	$SrHg_{11}$	$SrHg_8$
4	Sr_5Hg_{95}	single crystal	$SrHg_8$	$Sr_{10}Hg_{55}$
5	$Sr_{15}Hg_{85}$	single crystal	$Sr_{10}Hg_{55}$	$SrHg_8$
6	$Sr_{20}Hg_{80}$	single crystal	$Sr_{10}Hg_{55}$	$SrHg_2$
7	$Sr_{25}Hg_{75}$	polycrystalline	$Sr_{10}Hg_{55}$	$SrHg_3$
8	$Sr_{30}Hg_{70}$	polycrystalline	$SrHg_2$	$Sr_{10}Hg_{55}$
9	$Sr_{40}Hg_{60}$	polycrystalline	$SrHg_2$	Sr_3Hg_2
10	$Sr_{50}Hg_{50}$	polycrystalline	SrHg and Sr_3Hg_2	$SrHg_2$
11	$Sr_{63}Hg_{37}$	polycrystalline	SrHg	$SrHg_2$
12	$Sr_{67}Hg_{33}$	polycrystalline	Sr_3Hg	Sr_3Hg_2
13	$Sr_{70}Hg_{30}$	polycrystalline	Sr_3Hg_2	Sr_3Hg and SrHg
14	$Sr_{79}Hg_{21}$	polycrystalline	Sr_3Hg	SrHg

and physical properties of mercurides and amalgams by utilizing a set of dedicated experimental techniques (Leithe-Jasper et al., 2006).

All of the samples were synthesized by combining Hg (droplet, Alfa Aesar, 99.999%) and Sr (pieces, Alfa Aesar, 99.95%), with the Sr:Hg ratio varied from 2:98 to 79:21 (Table 1). Elements were sealed in tantalum tubes, in order to preserve stoichiometry. To protect samples from air and moisture, all syntheses were performed in an argon filled glove box system. The tubes were heated up to 500°C over 24 h and held there for a further 50 h before cooling back to room temperature over 96 h, with the slow cooling ensuring that the samples were able to crystallize efficiently. Mercury-rich samples were then placed into specialized crucibles (Canfield and Svanidze, 2024) (Figure 2) and centrifuged at room temperature to remove excess mercury. While most of the mercury can be eliminated this way, the small remainder can usually be removed by allowing the crystals to sit on gold foil for several days. Resultant single crystals of $SrHg_{11}$, $SrHg_8$, and $Sr_{10}Hg_{55}$ are shown in Figure 2 (bottom). The rest of the compounds were synthesized in polycrystalline form. It is important to note, that secondary phases were present in all samples (Table 1).

Powder X-ray diffraction was performed on a Huber G670 Image plate Guinier camera with a Ge-monochromator (Cu$K\alpha_1$, λ = 1.54056 Å). Powders were sealed between two Kapton films to prevent decomposition. Phase identification was carried out using WinXPow software (Darmstadt STOE and Cie GmbH, 2019). The lattice parameters were determined by a least-squares refinement using the peak positions, extracted by profile fitting. The WinCSD software (Akselrud and Grin, 2014) was used for crystallographic analysis. Single crystal diffraction was not carried out due to the extreme air-sensitivity of these materials. The values of the lattice parameters, refined from powder X-ray data, were in agreement with those reported previously (Table 2).

Differential thermal analysis (DTA) was performed using STA 449 F3 Jupiter (NETZSCH) and DCS 404 Pegasus (NETZSCH) set-ups with a 10 K/min heating and cooling rate. The samples were measured in the temperature range from 25°C to 875°C, with the exact ranges based on expected transitions. The previously published mercury-strontium binary phase diagram defined by (Gumiński, 2005) was used as a guide. Samples were sealed in tantalum ampoules, under argon. The particularly challenging part was to evaluate the mercury-rich samples, given their high vapor pressure – this region of the binary phase diagram is also the least explored one. For this, modified stainless steel high-pressure capsules with a volume of 30 μL from PerkinElmer were used (Figure 2). The sample masses were around 40–50 mg for DTA and 90–100 mg for DSC.

Magnetic properties were examined using a Quantum Design (QD) Magnetic Property Measurement System in the temperature range of 1.8–300 K and under various applied magnetic fields. Samples were sealed in glass tubes to prevent reaction with air. The specific heat data were collected on a QD Physical Property Measurement System from 0.4 K to 10 K and under various applied magnetic fields. Given the high air-sensitivity of the mercury-rich phases, samples were covered with Apiezon N vacuum grease, which resulted in a rather large background (Figure 3, panel a) – and while the transition to the superconducting state was observed, it was unfortunately not possible to carry out an in-depth analysis of the superconducting state. The corresponding H_{c2} – T phase diagrams were constructed and fit to Ginzburg–Landau

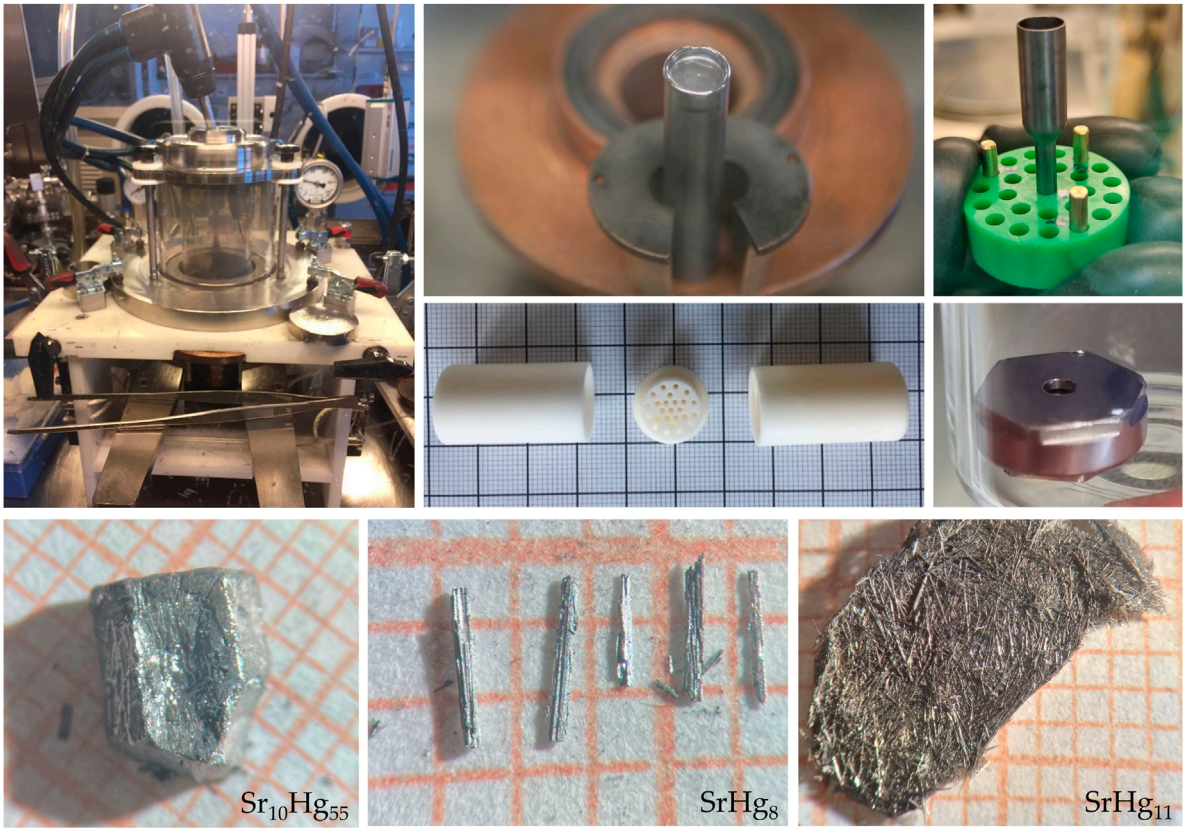

FIGURE 2
Top: Experimental solutions used for synthesis and characterization of mercury-strontium compounds. Left: arc melter used for sealing tantalum tubes under argon. Center, top: sealed tantalum tube. Center bottom: Canfield-Svanidze crucible set used for centrifugation of samples. Right, top: tantalum ampoule used for DTA measurements. Right, bottom: modified stainless steel high-pressure capsule used for DSC as an alternative to DTA on mercury-rich samples. Bottom: Single crystals of superconducting strontium mercurides–$SrHg_{11}$ (sample 1), $SrHg_8$ (sample 4), and $Sr_{10}Hg_{55}$ (sample 4, Table 1).

relation $H_{c2}(T) = H_{c2}(0)(1-(T/T_c)^2)/(1+(T/T_c)^2)$ describing the temperature dependence of the upper critical field H_{c2}. Given low critical temperatures, it was not possible to extract the values of lower critical field H_{c1}. The critical temperatures were extracted from the magnetic susceptibility and specific heat data by taking the mid-point of the superconducting transition. For $SrHg_8$ and $SrHg_{11}$, a significant variation of the T_c values can be explained by the presence of a homogeneity range (Table 2; Figure 3).

3 Results and discussion

As mentioned above, the goal of this work was to revisit the mercury-strontium phases and explore their physical properties. In order to clarify the phases and their evolution with temperature, a complementary analysis of the powder X-ray diffraction and differential thermal analysis was implemented. The following phases were examined: $SrHg_{11}$, $SrHg_8$, $Sr_{10}Hg_{55}$, $SrHg_2$, SrHg, Sr_3Hg_2, and Sr_3Hg. No evidence of $SrHg_3$ (Wendorff and Röhr, 2018) or Sr_2Hg (Bruzzone and Merlo, 1974; Gumiński, 2005) was found. The difficulty in stabilizing the former can perhaps be explained by a relatively short liquidus line (Wendorff and Röhr, 2018).

Motivated by the lack of publications addressing physical properties of strontium mercurides, we have performed a thorough analysis of these materials. Much like in our previous work (Witthaut et al., 2023; Prots et al., 2022a; Prots et al., 2022b; Svanidze et al., 2019), we have taken considerable care to protect our samples from decomposition in order to study their intrinsic properties. All of the phases from 25 at.% strontium and up, were found to be either dia- or paramagnetic down to the lowest measured temperature $T = 1.8$ K (not shown). However, for the mercury-rich samples, three new superconducting phases were identified – $SrHg_{11}$, $SrHg_8$, and $Sr_{10}Hg_{55}$. While all of these phases were grown in single crystal form, they contain some inclusions of secondary phases (Table 1). This explains why magnetization measurements, shown in Figure 3, show multiple transitions. Each of these transitions can be assigned to the respective phases, present in these samples – $SrHg_{11}$ ($T_c = 3.2 \pm 0.3$ K), $SrHg_8$ ($T_c = 3.0 \pm 0.1$ K), or $Sr_{10}Hg_{55}$ ($T_c = 2.2 \pm 0.25$ K). Uncertainties in T_c were determined by averaging the values obtained from various measurements and various samples. The majority and minority phases in each sample were identified *via* powder diffraction analysis. For the heat capacity data, a single anomaly is seen around $T = 2.2$ K, corresponding to the superconducting transition of $Sr_{10}Hg_{55}$. This transition is

10.3389/fmats.2024.1470878

TABLE 2 Properties of mercury-strontium phases, examined as part of this work.

Sample number	Phase	Space group, structure type	Lattice parameters (Previous reports)	Lattice parameters (Current work)	T_c (K)	H_c (T)
1, 2, 3	$SrHg_{11}$	$Pm\bar{3}m$, $BaHg_{11}$	a = 9.510 (2) Å	a = 9.4974(7) - 9.561(2) Å	3.2 ± 0.3	0.18 ± 0.05
			V = 860.14 Å^3	V = 856.67–873.97 Å^3		
			Biehl and Deiseroth (1999)			
2, 3, 4, 5	$SrHg_8$	*Pnma*, $SrHg_8$	a = 13.328 (1) Å	a = 13.2837(1) –13.3580(4) Å	3.0 ± 0.1	0.35 ± 0.02
			b = 4.9128 (5) Å	b = 4.9083(1) –4.9459(7) Å		
			c = 26.446 (3) Å	c = 26.367(1) –26.536(9) Å		
			V = 1731.63 Å^3	V = 1719.14–1748.49 Å^3		
			Tkachuk and Mar (2010)			
4, 5, 6, 8	$Sr_{10}Hg_{55}$	$P\bar{6}$, $Eu_{10}Hg_{55}$	a = 13.602 (2) Å	a = 13.6339(2) –13.776(2) Å	2.2 ± 0.25	0.54 ± 0.05
			c = 9.818 (1) Å	c = 9.8529(5) - 9.947(2) Å		
			V = 1573.11 Å^3	V = 1586.68–1634.46 Å^3		
			Tkachuk and Mar (2008)			
8, 9, 10, 11	$SrHg_2$	*Imma*, $CeCu_2$	a = 4.985 Å	a = 4.938(1)–5.0003(4) Å	–	–
			b = 7.754 Å	b = 7.748(2)–7.7800(5) Å		
			c = 8.550 Å	c = 8.5127(5)–8.634(9) Å		
			V = 330.49 Å^3	V = 328.46–333.49 Å^3		
			Bruzzone and Merlo (1974)			
10, 11	SrHg	$Pm\bar{3}m$, CsCl	a = 3.955 Å	a = 3.9458(2)–3.9530(1) Å	–	–
			V = 61.83 Å^3	V = 61.43–61.77 Å^3		
			Bruzzone and Merlo (1974)			
9, 10, 12	Sr_3Hg_2	*P4mbm*, U_3Si2	a = 8.877 Å	a = 8.887(1)–9.020(1) Å	–	–
			c = 4.556 Å	c = 4.5538(7)–4.568(1) Å		
			V = 359.02 Å^3	V = 360.00–371.66 Å^3		
			Bruzzone and Merlo (1974)			
12, 14	Sr_3Hg	*Pnma*, Fe_3C	a = 11.08 Å	a = 11.044(3)–11.192(2) Å	–	–
			b = 7.405 Å	b = 7.359(2)–7.380(1) Å		
			c = 8.523 Å	c = 8.571(1)–8.578(2) Å		
			V = 699.29 Å^3	V = 697.13–708.00 Å^3		
			Bruzzone and Merlo (1974)			

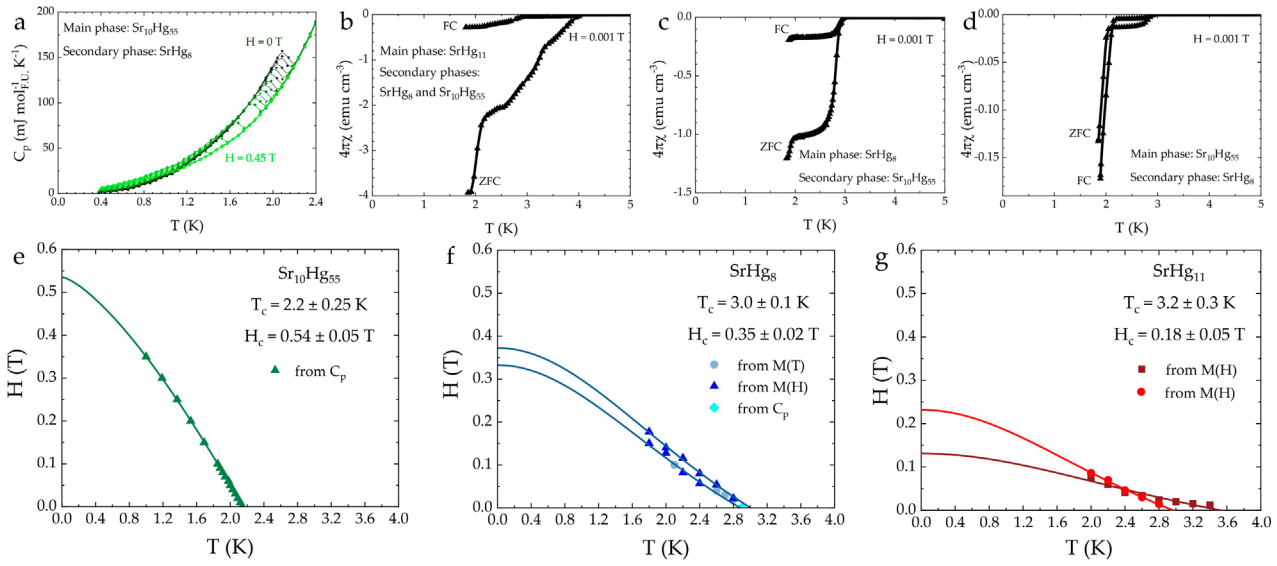

FIGURE 3
Superconducting properties of strontium mercurides $Sr_{10}Hg_{55}$, $SrHg_8$, and $SrHg_{11}$. **(A)** Specific heat for $Sr_{10}Hg_{55}$ **(B–D)** Magnetic susceptibility for the three superconducting samples, each panel shows one sample which has multiple superconducting transitions. Both ZFC (zero-field-cooled) and FC (field-cooled) curves are shown. **(E–G)** $H-T$ phase diagrams constructed from the heat capacity and magnetic measurements, from which the values of T_c and H_{c2} can be extracted. For $SrHg_8$ and $SrHg_{11}$, variation in stoichiometry from sample to sample yields slightly different T_c values.

driven to lower temperatures as magnetic field is increased, in accordance with what is expected for a superconductor. Based on the joint analysis of magnetic susceptibility and specific heat data, the $H-T$ phase diagrams were constructed for $SrHg_{11}$, $SrHg_8$, and $Sr_{10}Hg_{55}$. By fitting the data to the Ginzburg–Landau relation, as shown in Figure 3 (bottom), values of the respective $T_c(0)$ and $H_{c2}(0)$ were extracted, as summarized in Table 2. For $SrHg_8$ and $SrHg_{11}$, there appears to exist a range of values for both T_c and H_{c2}. This can likely be attributed to a presence of the homogeneity range of these materials, as deduced by slight variation of the lattice parameters, summarized in Table 2. The presence of a homogeneity range in the $Sr_{11-x}Hg_{54+x}$ compound was previously reported to arise from disorder resulting from mixing of Sr and Hg on the same crystallographic position (Tkachuk and Mar, 2008). This, in fact, is rather common for this structure type – similar disorder has been observed in $Eu_{11-x}Hg_{54+x}$ (Tambornino and Hoch, 2015; Zaremba et al., 2024), which is isostructural to $Sr_{11-x}Hg_{54+x}$. The exact mechanism of change in stoichiometry between different samples of $SrHg_8$ and $SrHg_{11}$ is less clear. For $SrHg_8$, single crystal X-ray diffraction analysis did not reveal any disorder present (Tkachuk and Mar, 2010). For $SrHg_{11}$, only powder X-ray diffraction data was previously analyzed (Biehl and Deiseroth, 1999). In general, in complex compounds with mercury, chemical disorder is enabled by a large number of possible positions for mercury as well as other elements (Svanidze et al., 2019; Tambornino et al., 2015). Crystal structures of both $SrHg_8$ and $SrHg_{11}$ are rather complex and have many crystallographic sites. However, in the current study, it was not possible to carry out single crystal diffraction experiments, which could perhaps elucidate the mechanism(s) behind the variation of the lattice parameters in $SrHg_8$ and $SrHg_{11}$.

It is important to note that the values of the upper critical fields H_{c2} for $SrHg_{11}$, $SrHg_8$, and $Sr_{10}Hg_{55}$ are about an order of magnitude larger than those observed for other conventional, BCS-type mercury-based superconductors such as $LaHg_{6.4}$ (H_{c2} = 0.061 T (Prots et al., 2022a)), Lu/$ScHg_3$ (H_{c2} = 0.08 T (Witthaut et al., 2023)), as well as elemental Hg (H_{c2} = 0.04 T (Finnemore et al., 1960)). However, given that for all three compounds the values of H_{c2} are significantly below the Pauli limit (Clogston, 1962; Chandrasekhar, 1962) (4.09 T for $Sr_{10}Hg_{55}$, 5.58 T for $SrHg_8$, and 5.95 T for $SrHg_{11}$), it is most likely that the superconductivity of these materials is conventional. Typically, the values of the specific heat jump, as well as the electron-phonon coupling constant can be extracted from the specific heat data, which in this case was not possible. Another argument in favor of conventional superconductivity of strontium mercurides is the robustness of superconductivity to the crystallographic disorder. However, further investigations of the superconducting strontium mercurides, in particular $Sr_{10}Hg_{55}$, are of interest, given the noncentrosymmetric crystal structure of this compound. Superconductors that lack inversion symmetry can often host a variety of peculiar phenomena (Naskar et al., 2021; Tanaka et al., 2023; Chirolli et al., 2022; Smith et al., 2021), even if their critical temperatures and fields are relatively low. As we have shown previously, a complementary analysis of specific heat and muon spin relaxation, rotation, and resonance (μSR) can be used to comprehensively understand these systems (Khasanov et al., 2020a; Khasanov et al., 2020b; Beare et al., 2019; Amon et al., 2018).

4 Conclusion

The mercury-strontium compounds were revisited with the emphasis on the mercury-rich phases for two reasons: (i) conflicting reports regarding existing phases and (ii) a possibility of finding new superconductors. The reformulation of the system was made

possible by implementing differential thermal analysis coupled with powder X-ray diffraction experiments. Existence of $SrHg_{11}$, $SrHg_8$, $Sr_{10}Hg_{55}$, $SrHg_2$, SrHg, Sr_3Hg_2, and Sr_3Hg was confirmed.

The physical properties of all phases were probed down to $T = 1.8$ K. While the majority of strontium mercurides are paramagnetic or diamagnetic, three new superconductors have been identified: $SrHg_{11}$ ($T_c = 3.2 \pm 0.3$ K, $H_{c2} = 0.18 \pm 0.05$ T), $SrHg_8$ ($T_c = 3.0 \pm 0.1$ K, $H_{c2} = 0.35 \pm 0.02$ T), and $Sr_{10}Hg_{55}$ ($T_c = 2.2 \pm 0.25$ K, $H_{c2} = 0.54 \pm 0.05$ T). While the critical fields are higher than those of other mercury-based superconductors, the superconductivity of $SrHg_{11}$, $SrHg_8$, and $Sr_{10}Hg_{55}$ is likely conventional. However, future investigations of the superconducting state in $Sr_{10}Hg_{55}$ by means of muon spin relaxation, rotation, and resonance is warranted, given its noncentrosymmetric crystal structure.

Data availability statement

The original contributions presented in the study are included in the article/supplementary material, further inquiries can be directed to the corresponding author.

Author contributions

RN: Conceptualization, Data curation, Methodology, Visualization, Writing–original draft, Writing–review and editing. YP: Data curation, Investigation, Methodology, Writing–review and editing. MK: Data curation, Investigation, Methodology, Visualization, Writing–review and editing. NZ: Data curation, Investigation, Methodology, Writing–review and editing. OP: Data curation, Writing–review and editing. MS: Data curation, Investigation, Methodology, Writing–review and editing. LA: Data curation, Investigation, Writing–review and editing. YG: Data curation, Investigation, Methodology, Writing–review and editing. ES: Conceptualization, Data curation, Funding acquisition, Investigation, Methodology, Project administration, Supervision, Validation, Writing–original draft, Writing–review and editing.

Funding

The author(s) declare that financial support was received for the research, authorship, and/or publication of this article. Open access funded by Max Planck Society. RN and ES acknowledge the funding from the International Max Planck Research School for Chemistry and Physics of Quantum Materials and the funding provided by the German Research Foundation (DFG-528628333 "Complex compounds based on mercury"). OP acknowledges financial support from the Polish National Agency for Academic Exchange (NAWA) under the Bekker programme (BPN/BEK/2022/1/00190/U/00001).

Conflict of interest

The authors declare that the research was conducted in the absence of any commercial or financial relationships that could be construed as a potential conflict of interest.

Publisher's note

References

Akselrud, L., and Grin, Y. (2014). WinCSD: software package for crystallographic calculations (Version 4). *J. Appl. Crystallogr.* 47, 803–805. doi:10.1107/s1600576714001058

Amon, A., Svanidze, E., Cardoso-Gil, R., Wilson, M. N., Rosner, H., Bobnar, M., et al. (2018). Noncentrosymmetric superconductor BeAu. *Phys. Rev. B* 97, 014501. doi:10.1103/PhysRevB.97.014501

Beare, J., Nugent, M., Wilson, M., Cai, Y., Munsie, T., Amon, A., et al. (2019). muSR and magnetometry study of the type-I superconductor BeAu. *Phys. Rev. B* 99, 134510. doi:10.1103/physrevb.99.134510

Biehl, E., and Deiseroth, H. J. (1999). Preparation, structural relations, and magnetism of amalgams MHg_{11} (M: K, Rb, Ba, Sr). *Z. fur Anorg. Allg. Chem.* 625, 1073–1080. doi:10.1002/CHIN.199938008

Bjørklund, G. (1989). The history of dental amalgam. *Tidsskr. Nor. Laegeforen* 109 (34-36), 3582–3585.

Bjørklund, G., Dadar, M., Mutter, J., and Aaseth, J. (2017). The toxicology of mercury: current research and emerging trends. *Environ. Res.* 159, 545–554. doi:10.1016/j.envres.2017.08.051

Bruzzone, G., and Merlo, F. (1973). The calcium-mercury system. *J. Less-Common Metals* 32, 237–241. doi:10.1016/0022-5088(73)90091-X

Bruzzone, G., and Merlo, F. (1974). The strontium-mercury system. *J. Less Common Metals* 35, 153–157. doi:10.1016/0022-5088(74)90154-4

Bruzzone, G., and Merlo, F. (1975). The barium-mercury system. *J. Less-Common Metals* 39, 271–276. doi:10.1016/0022-5088(75)90201-5

Canfield, P., and Svanidze, E. (2024). *Canfield-Svanidze crucible sets*. LSP Industrial Ceramics, Inc. Available at: https://www.lspceramics.com/canfield-svanidze-crucibles/.

Chandrasekhar, B. S. (1962). A note on the maximum critical field of high-field superconductors. *Appl. Phys. Lett.* 1, 7–8.

Chirolli, L., Mercaldo, M. T., Guarcello, C., Giazotto, F., and Cuoco, M. (2022). Colossal orbital edelstein effect in noncentrosymmetric superconductors. *Phys. Rev. Lett.* 128, 217703. doi:10.1103/physrevlett.128.217703

Claeson, T., and Luo, H. L. (1966). Superconducting transition temperatures of mercury-alkaline earth metal compounds. *J. Phys. Chem. solids* 27, 1081–1085. doi:10.1016/0022-3697(66)90083-7

Clogston, A. M. (1962). Upper limit for the critical field in hard superconductors. *Phys. Rev. Lett.* 9, 266–267.

Conrad, M., Harbrecht, B., Weber, T., Jung, D. Y., and Steurer, W. (2009). Large, larger, largest–a family of cluster-based tantalum copper aluminides with giant unit cells. ii. the cluster structure. *Acta Crystallogr. Sect. B Struct. Sci.* 65, 318–325. doi:10.1107/s0108768109014013

Darmstadt STOE and Cie GmbH (2019). *Winxpow*.

Devoto, G., and Recchia, E. (1930). The Sr amalgam. *Gazz. Chim. Ital.* 60, 688–692.

Druska, C., Doert, T., and Böttcher, P. (1996). Refinement of the crystal structure of Sr_3Hg_2. *Z. fur Anorg. Allg. Chem.* 622, 401–404. doi:10.1002/zaac.19966220304

Dubois, J.-M., and Belin-Ferré, E. (2010). *Complex metallic alloys*.

Ferro, R. (1954). The crystal structures of SrCd, BaCd, SrHg and BaHg. *Acta Cryst.* 7, 781. doi:10.1107/s0365110x5400240x

Finnemore, D., Mapother, D., and Shaw, R. (1960). Critical field curve of superconducting mercury. *Phys. Rev.* 118, 127–129. doi:10.1103/physrev.118.127

Gumiński, C. (2005). The Hg-Sr (mercury-strontium) system. *J. Phase Equilibria Diffusion* 26, 81–86. doi:10.1361/15477030522590

Guntz, A., and Roederer, G. (1906). Sur les amalgames de strontium. *Bull. Soc. Chim. Fr.* 35, 494–503.

Hänisch, J., Wimbush, S. C., Berger, L. I., and Roberts, B. W. (2023). "Properties of superconductors," in *CRC handbook of chemistry and physics*. Editor J. R. Rumble (Boca Raton, FL: CRC Press/Taylor and Francis).

Hoch, C. (2019). Mein lieblingselement: quecksilber. *Nachrichten aus Chem.* 67, 54–60. doi:10.1002/nadc.20194090184

Hohl, T., Kremer, R. K., Ebbinghaus, S. G., Khan, S. A., Minár, J., and Hoch, C. (2023). Influence of disorder on the bad metal behavior in polar amalgams. *Inorg. Chem.* 62, 3965–3975. doi:10.1021/acs.inorgchem.2c04430

Kerp, W. (1898). Zur kenntnis der amalgame. *Z. Anorg. Chem.* 17, 284–309. doi:10.1002/zaac.18980170129

Kerp, W., Böttger, W., and Iggena, H. (1900). On the knowledge of amalgams. *Z. Anorg. Chem.* 25, 1–71. doi:10.1002/zaac.19000250102

Khasanov, R., Gupta, R., Das, D., Amon, A., Leithe-Jasper, A., and Svanidze, E. (2020a). Multiple-gap response of type-I noncentrosymmetric BeAu superconductor. *Phys. Rev. Res.* 2, 023142. doi:10.1103/physrevresearch.2.023142

Khasanov, R., Gupta, R., Das, D., Leithe-Jasper, A., and Svanidze, E. (2020b). Single-gap versus two-gap scenario: specific heat and thermodynamic critical field of the noncentrosymmetric superconductor BeAu. *Phys. Rev. B* 102, 014514. doi:10.1103/physrevb.102.014514

König, M., Wiedmann, S., Brüne, C., Roth, A., Buhmann, H., Molenkamp, L. W., et al. (2007). Quantum spin hall insulator state in HgTe quantum wells. *Sci.* 45, 766–770. doi:10.1126/science.1148047

Leithe-Jasper, A., Borrmann, H., and Hönle, W. (2006). *Max Planck Institute for chemical Physics of solids, scientific report*. Dresden: Max-planck-gesellschaft.

Naskar, M., Mishra, P., Ash, S., and Ganguli, A. (2021). Superconductors with noncentrosymmetric crystal structures. *Bull. Mater. Sci.* 44, 278. doi:10.1007/s12034-021-02587-z

Pelloquin, D., Hervieu, M., Michel, C., Tendeloo, G. V., Maignan, A., and Raveau, B. (1993). A 94 K Hg-based superconductor with a "1212" structure $Hg_{0.5}Bi_{0.5}Sr_2Ca_{1-x}R_xCu_2O_{6+\delta}$ (R=Nd, Y, Pr). *Phys. C Supercond. its Appl.* 216, 257–263. doi:10.1016/0921-4534(93)90069-3

Prots, Y., Krnel, M., Grin, Y., and Svanidze, E. (2022a). Superconductivity in crystallographically disordered $LaHg_{6.4}$. *Inorg. Chem.* 61, 15444–15451. doi:10.1021/acs.inorgchem.2c01987

Prots, Y., Krnel, M., Schmidt, M., Grin, Y., and Svanidze, E. (2022b). Uranium-mercury complex antiferromagnet: $UHg_{6.4}$. *Phys. Rev. B* 106, L060412. doi:10.1103/PhysRevB.106.L060412

Roberts, B. W. (1976). Survey of superconductive materials and critical evaluation of selected properties. *J. Phys. Chem. reference data* 5, 581–822. doi:10.1063/1.555540

Samson, S. (1962). Crystal structure of $NaCd_2$. *Nature* 195, 259–262. doi:10.1038/195259a0

Sappl, J., Freund, R., and Hoch, C. (2017). Stuck in our teeth? crystal structure of a new copper amalgam, Cu_3Hg. *Crystals* 7, 352. doi:10.3390/cryst7120352

Smith, M., Andreev, A., and Spivak, B. (2021). Giant magnetoconductivity in noncentrosymmetric superconductors. *Phys. Rev. B* 104, L220504. doi:10.1103/physrevb.104.l220504

Steurer, W., and Dshemuchadse, J. (2016). *Intermetallics: structures, properties, and statistics, vol. 26*. Oxford University Press.

Svanidze, E., Amon, A., Borth, R., Prots, Y., Schmidt, M., Nicklas, M., et al. (2019). Empirical way for finding new uranium-based heavy-fermion materials. *Phys. Rev. B* 99, 220403R. doi:10.1103/physrevb.99.220403

Tambornino, F., and Hoch, C. (2015). The mercury-richest europium amalgam $Eu_{10}Hg_{55}$. *Z. fur Anorg. Allg. Chem.* 641, 537–542. doi:10.1002/zaac.201400561

Tambornino, F., Sappl, J., and Hoch, C. (2015). The $Gd_{14}Ag_{51}$ structure type and its relation to some complex amalgam structures. *J. Alloys Compd.* 618, 326–335. doi:10.1016/j.jallcom.2014.08.017

Tanaka, H., Watanabe, H., and Yanase, Y. (2023). Nonlinear optical responses in noncentrosymmetric superconductors. *Phys. Rev. B* 107, 024513. doi:10.1103/physrevb.107.024513

Tkachuk, A. V., and Mar, A. (2008). Alkaline-earth metal mercury intermetallics $A_{11-x}Hg_{54+x}$ (A = Ca, Sr). *Inorg. Chem.* 47, 1313–1318. doi:10.1021/ic7015148

Tkachuk, A. V., and Mar, A. (2010). In search of the elusive amalgam $SrHg_8$: a mercury-rich intermetallic compound with augmented pentagonal prisms. *Dalton Trans.* 39, 7132–7135. doi:10.1039/c0dt00304b

Urban, K., and Feuerbacher, M. (2004). Structurally complex alloy phases. *J. non-crystalline solids* 334, 143–150. doi:10.1016/j.jnoncrysol.2003.11.029

Weber, T., Dshemuchadse, J., Kobas, M., Conrad, M., Harbrecht, B., and Steurer, W. (2009). Large, larger, largest–a family of cluster-based tantalum copper aluminides with giant unit cells. i. structure solution and refinement. *Acta Crystallogr. Sect. B Struct. Sci.* 65, 308–317. doi:10.1107/s0108768109014001

Wendorff, M., and Röhr, C. (2018). Alkaline-earth tri-mercurides $AIIHg_3$ (AII=Ca, Sr, Ba): binary intermetallic compounds with a common and a new structure type. *Z. fur Kristallogr. - Cryst. Mater.* 233, 515–529. doi:10.1515/zkri-2018-2054

Witthaut, K., Prots, Y., Zaremba, N., Krnel, M., Leithe-Jasper, A., Grin, Y., et al. (2023). Chemical and physical properties of YHg_3 and $LuHg_3$. *ACS Org. Inorg. Au* 3, 143–150. doi:10.1021/acsorginorgau.2c00048

Zaremba, N., Krnel, M., Prots, Y., Sichelschmidt, J., Brando, M., Akselrud, L., et al. (2024). *Magnetic properties of $Eu_{10}Hg_{55}$. in preparation*.